AD-A047 315 HUGHES RESEARCH LABS MALIBU CALIF F/G 20/6
COMPONENTS FOR SINGLE STRAND MULTIMODE FIBER SYSTEMS.(U)
AUG 77 M BARNOSKI, B CHEN, H R FRIEDRICH F19628-77-C-0103
UNCLASSIFIED RADC-TR-77-284 NL

OF
AD
A047315

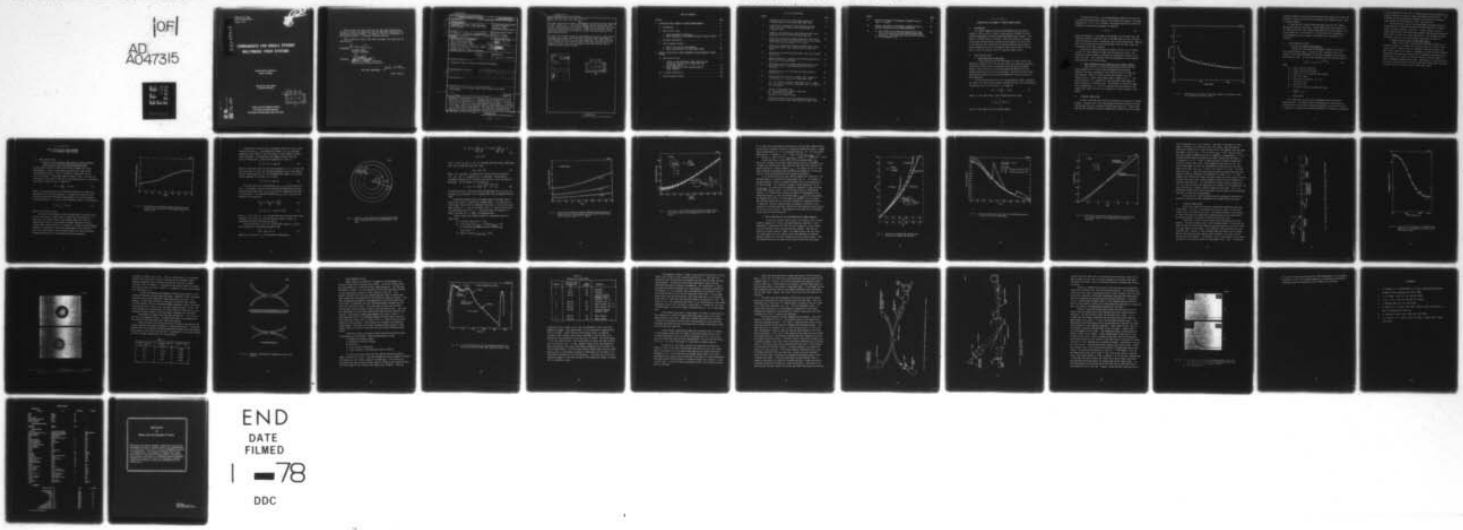

END
DATE
FILMED
1 -78
DDC

RADC-TR-77-284
Interim Technical Report
August 1977

AD A047315

COMPONENTS FOR SINGLE STRAND MULTIMODE FIBER SYSTEMS

Hughes Research Laboratories
Malibu, CA 90265

Approved for public release;
distribution unlimited.

DDC
RECEIVED
DEC 6 1977
D

ROME AIR DEVELOPMENT CENTER
AIR FORCE SYSTEMS COMMAND
GRIFFISS AIR FORCE BASE, NEW YORK 13441

AD No.____
DDC FILE COPY

This report has been reviewed by the RADC Information Office (OI) and is releasable to the National Technical Information Service (NTIS). At NTIS it will be releasable to the general public, including foreign nations.

This technical report has been reviewed and approved for publication.

APPROVED: Richard Payne

RICHARD PAYNE
Project Engineer

APPROVED: Robert M. Barrett

ROBERT M. BARRETT, Director
Solid State Sciences Division

FOR THE COMMANDER: John P. Huss

Plans Office

UNCLASSIFIED

SECURITY CLASSIFICATION OF THIS PAGE (When Data Entered)

(19) REPORT DOCUMENTATION PAGE	READ INSTRUCTIONS BEFORE COMPLETING FORM
(10) 1. REPORT NUMBER: RADC-TR-77-284	2. GOVT ACCESSION NO. / 3. RECIPIENT'S CATALOG NUMBER
(6) 4. TITLE (and Subtitle): COMPONENTS FOR SINGLE STRAND MULTIMODE FIBER SYSTEMS	5. TYPE OF REPORT & PERIOD COVERED: Scientific Report 1 1/3/77 to 7/3/77
	6. PERFORMING ORG. REPORT NUMBER
(10) 7. AUTHOR(s): M. Barnoski, B. Chen, H. R. Friedrich, S. Jensen, E. Marom, O. G. Ramer, M. Rourke, H. Ten	(15) 8. CONTRACT OR GRANT NUMBER(s): F19628-77-C-0103 New
9. PERFORMING ORGANIZATION NAME AND ADDRESS: Hughes Research Laboratories, 3011 Malibu Canyon Road, Malibu, California 90265	10. PROGRAM ELEMENT, PROJECT, TASK AREA & WORK UNIT NUMBERS: 61102F, (16) 2306J221 (17) J2
11. CONTROLLING OFFICE NAME AND ADDRESS: Deputy for Electronic Technology (RADC), Hanscom AFB, MA 01731, Contract Monitor: Richard Payne/ESO	(11) 12. REPORT DATE: Aug [redacted] 77
	13. NUMBER OF PAGES: 39
14. MONITORING AGENCY NAME & ADDRESS(if different from Controlling Office) (12) 41 p.	15. SECURITY CLASS. (of this report): UNCLASSIFIED
	15a. DECLASSIFICATION DOWNGRADING SCHEDULE

16. DISTRIBUTION STATEMENT (of this Report)

Approved for public release; distribution unlimited.

17. DISTRIBUTION STATEMENT (of the abstract entered in Block 20, if different from Report)

(9) Scientific rpt. no. 1, 2 Jan – 2 Jul 77

18. SUPPLEMENTARY NOTES

19. KEY WORDS (Continue on reverse side if necessary and identify by block number)

Fiber Optics, Access Coupler, Mode Mixing, Optical Time Domain Reflectometer

20. ABSTRACT (Continue on reverse side if necessary and identify by block number)

~~We report~~ the development of a technique for the determination of the geometrical characteristics of a taper pulled in a fiber. This technique uses the deflection of a light beam due to the taper. The insertion loss of a taper has been experimentally investigated as a function of the modal index of the fiber both with the taper immersed in air and a high index fluid (diiodomethane). The results of these experiments show that the higher order modes are more easily out-coupled by the

IS DESCRIBED IN THIS REPORT

DD FORM 1 JAN 73 1473 EDITION OF 1 NOV 65 IS OBSOLETE

UNCLASSIFIED

SECURITY CLASSIFICATION OF THIS PAGE (When Data Entered)

172 600

taper than the lower order modes.

We report that the time domain reflectometer resolution has been increased to the 1 nanosec goal. This system has been used to measure the fiber losses; these losses are the same as obtained by the insertion loss technique at the measurement wavelengths. Fibers known to contain defects have been measured on this system to increase our understanding of the backscattering return.

We report the progress toward the development of CO_2 laser fused couplers. Although many couplers have been made, the experimental development of the fabrication technique has not been completed. The lowest insertion loss, highest tap ratio couplers made to date have been obtained by the lapping of fibers such that the lapped and polished sections can be either welded or epoxied together.

ACCESSION for
NTIS White Section
DDC Buff Section
UNANNOUNCED
JUSTIFICATION
BY
DISTRIBUTION/AVAILABILITY CODES
Dist. AVAIL. and/or SPECIAL
A

DDC
RECEIVED
DEC 6 1977
D

TABLE OF CONTENTS

LIST OF ILLUSTRATIONS

S E C T I O N I

INTRODUCTION AND SUMMARY OF MAJOR ACCOMPLISHMENTS

A. INTRODUCTION

This report summarizes the work performed during the period January 3, 1977 to July 31, 1977, on the contract (F19628-77-C-0103) entitled "Components for Single Strand Multimode Fiber Systems." The report is divided into two sections. The first section is a summary of the major accomplishments achieved on the program since the start of the contract; the second section contains detailed description of work performed during the 3rd bimonthly report period (May 3, 1977 to July 3, 1977) and outlines plans for the next report period.

B. TAPER COUPLER STUDY

1. Taper measurement techniques

To optimize the coupling efficiency of a taper coupler the geometrical characteristics of the taper need to be measured accurately. The low loss fiber is very transparent and of cylindrical geometry making it very difficult to accurately determine dimensions of the tapered sections with an optical microscope. During this study a novel technique for determining the desired geometrical characteristics has been developed.

It has been established that if a narrow beam of light illuminates the taper, the light which propagates through the fiber will be deflected. The paraxial angle of deflection, μ, is given by

$$\sin \mu = 2 \left(\frac{\bar{n}}{n_o} - 1\right) \tan \alpha \qquad (1)$$

where α is the taper-angle, $\bar{n}$ the average refractive index

$$\bar{n} = \frac{1}{2r} \int_{-r}^{r} n(\rho)\, d\rho \qquad (2)$$

and n_o is the index of the surrounding medium.

The deflection angle μ can be determined by measuring the position of the deflected beam with respect to the diffraction pattern of the beam entrance slit. For a slit of width b, the angular position of the zero's (minima) of the diffraction pattern is given by

$$\mu = N \lambda/b \qquad (3)$$

where the integer N is the order of the minima. On the other hand, the light which passes around the fiber is not deflected, and the classical case of diffraction from a rectangular stop is again encountered. Measurement of the minima position and the distance from the fiber allows the calculation of the fiber diameter.

During this reporting period the optical analysis of the tapered section has been extended to other than the paraxial region. The analytical results suggest a technique for probing the internal structure of a fiber. This technique involves measurement of the intensity distribution of the deflected beam.

2. Modal dependence of the insertion loss of taper couplers.

Taper couplers can provide input/output coupling for full duplex operation on a single strand multimode fiber waveguide. Therefore the modal dependence of the insertion loss of a taper has been measured. When the tapered section was exposed to air the transmission of a taper versus modal index is shown in Fig. 1. The general behavior is as expected in that the higher order modes are more susceptible to radiation loss. The effect of covering the taper with diiodomethane (n = 1.74) is to increase the out coupling of the higher order modes; this will be discussed in a later section of this report.

C. T-COUPLER FABRICATION

Couplers have been fabricated for evaluation using several different methods. Standard fiber, with the protective overcoat removed, has been used to make straight, curved and twisted fused junctions. Fibers which have had the protective coating stripped and a portion of the core and/or

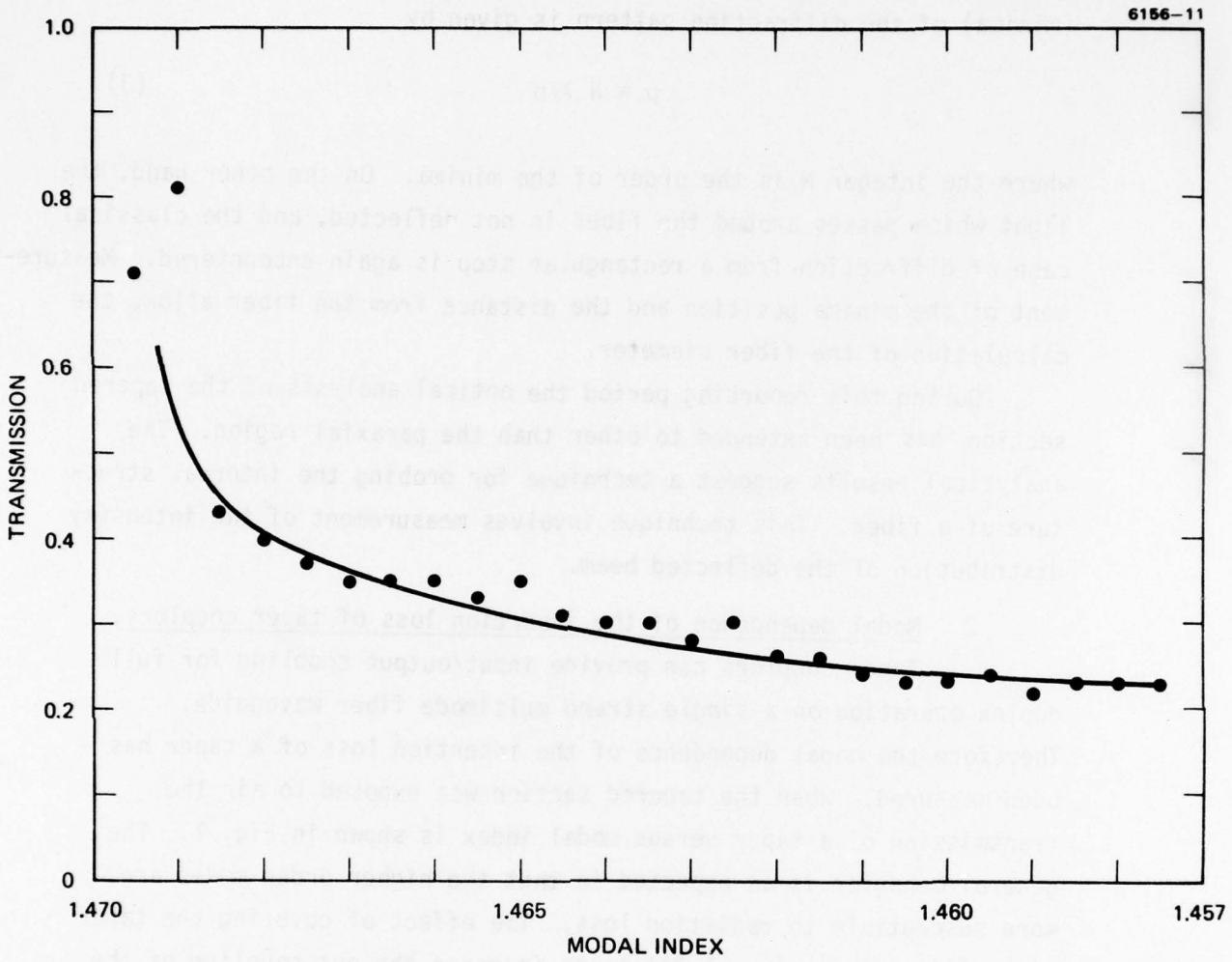

Fig. 1. Transmission efficiency of the taper coupler for different modes in a multimode step-index fiber.

cladding removed by lapping and polishing have also been used to fabricate junctions. These junctions have either been fused together using a laser or epoxied together.

To date the best couplers have been made using the LPE (lapped, polished and epoxied) technique. These couplers have lower excess loss for higher tap ratios than obtained from other fabrication methods. Due to the simplicity of construction it is felt that this technique will give repeatable results; however, sufficient data is presently not available.

D. FIBER PARAMETER STUDIES

1. Optical Time Domain Reflectometer

The optical time domain reflectometer (OTDR) was described in the second bimonthly report. Basically this instrument allows the display of the length dependence of the fiber attenuation by analyzing backscattered light. An analytical expression for the detected power is

$$P_d(z) = c_{in}\, c_o\, k\, s\, e^{-2\bar{\alpha}_T z}\, P_o \qquad (4)$$

where

c_{in} = input coupling efficiency
c_o = output coupling efficiency
k = insertion loss of tapered fiber coupler
P_o = peak laser power
$\bar{\alpha}_T$ = mean total attenuation = $\alpha_s + \alpha_a$
α_s = scattering loss
α_a = absorption loss
z = position of the pulse within the fiber
$s = \left(\frac{N.A.}{2n}\right)^2 \alpha_s \frac{c}{n} \tau$
τ = pulse width

This instrument has been used to determine fiber attenuation characteristics. The method offers the advantage of requiring access to only one end of the fiber and does not require that the fiber be cut. In addition, by inspecting the return waveform it is possible to determine

if the attenuation of the fiber is indeed constant and to determine the distance required to achieve a steady state modal distribution.[1] The technique can also be employed to measure the location of connectors and/or faults and the magnitude of their insertion loss.

The taper coupler used in these experiments provides sufficient directionality to eliminate the need for either electrical or optical gating to prevent detector saturation. It does, however, launch a rather complex modal distribution which affects the measured attenuation coefficient in fibers with little mode mixing. This problem has been overcome by the use of the mode scrambler described in report #2.

2. Modal characteristics of step index fibers

Modes in step index fibers may be selectively coupled to by varying the angle of incidence of the optical beam or by using a glass coupling prism. Mode mixing will ultimately limit the distance over which these signals will remain in the modes in which they were launched. Experiments have shown that mode mixing in commercially available step index fibers is very small and may not severely limit the length of a modally dependent communication system. Experiments to study the effect of a fiber splice on mode mixing have shown that a good splice should not introduce any serious mode mixing in step index fibers.

S E C T I O N I I

DETAIL DISCUSSION OF WORK PERFORMED IN 3RD BIMONTHLY REPORT PERIOD

A. TAPER COUPLER STUDY

1. Effects of the refraction index profile on the scattering (deflection) of light from side-illuminated tapers.

As described in previous reports (#1 and #2), diameter and slope measurements of tapers can be made by observing the light pattern obtained when a beam of light is incident at right angles to the axis of the taper. It has been shown in report #1 that a paraxial ray impinging at right angle to the axis of the tapered section is deflected by an angle μ given by (Eq. 5, report #1).

$$\sin \mu = 2\left(\frac{n}{n_o} - 1\right) \tan \alpha \qquad (1)$$

where α is the taper-angle, n the refractive index of the fiber and n_o the index of the surrounding medium. In report #2 the case of clad fibers with arbitrary refractive index profile, $n(\rho)$, was considered. It was shown that eq. (1) holds if the refractive index n is replaced by

$$\bar{n} = \frac{1}{2r} \int_{-r}^{r} n(\rho)\, d\rho \qquad (2)$$

where r is the fiber radius.

These derivations however, have only been made for paraxial rays, and the experimental evidence (Fig. 2) shows that the deflection is a function of the azimuth angle of the outgoing beam; this angle is measured with respect to the original incident light beam direction. In this report the deflection as a function of incident ray position and direction is evaluated. Since it has been shown in the literature [2-5] that a ray trace analysis gives accurate results for fiber scattering problems the evaluation is performed using the ray approach.

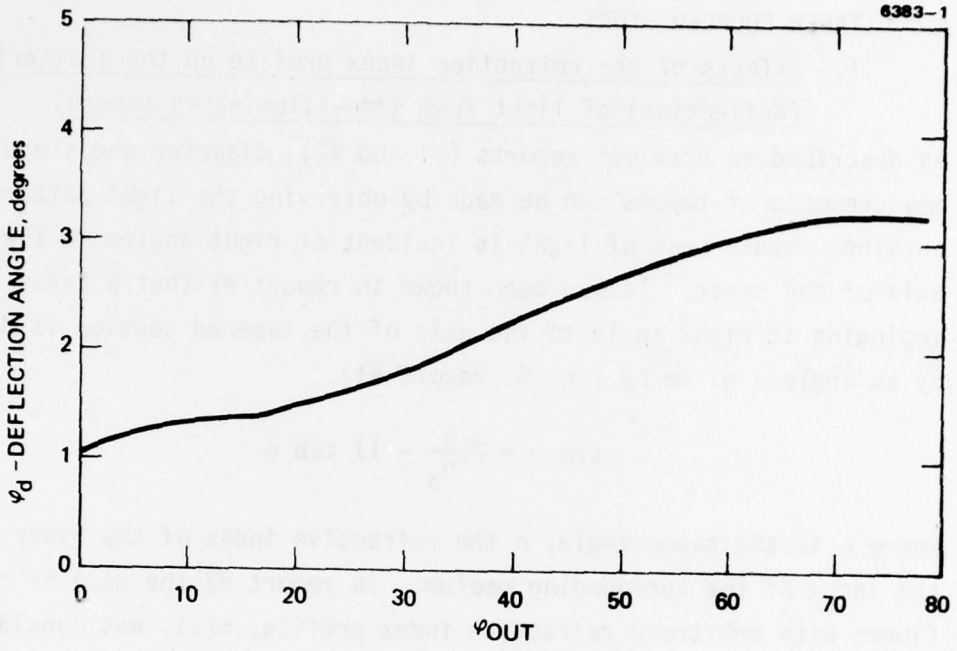

Fig. 2. Experimentally determined lateral deflection angle versus the azimuth angle of the outgoing beam for a tapered fiber.

Consider the original fiber as concentric shells of radia r_m and refractive indices n_m. Upon generating a taper, all cross-sectional dimensions scale linearly, while the values of the refractive indices remain unchanged. The envelope of the tapered section (near the point of inflection) is given by the equation of a cone, i.e.

$$\tilde{x}^2 + \tilde{y}^2 = (R - \tilde{z} \tan \alpha)^2 \tag{3}$$

where R is the outer radius of the cross section at $\tilde{z} = 0$, α is half the apex angle and $\tilde{x}$, $\tilde{y}$ and $\tilde{z}$ are the three orthogonal axes of the tapered region. Normalizing the $\tilde{x}$, $\tilde{y}$, $\tilde{z}$ coordinates with respect to R one gets for the envelope of the taper (i.e. a cone)

$$x^2 + y^2 = (1 - z \tan \alpha)^2 \tag{4}$$

Once the initial ray starting point (x_1, y_1, z_1) and direction $\vec{b}$ ($|b| = 1$) are known, the ray tracing consists of determining the intersection with the next shell (x_2, y_2, z_2) and the propagation direction $\vec{c}$ in this shell. The intersection point (x_2, y_2, z_2) is given by the solution of the equations

$$\frac{x_2 - x_1}{b_1} = \frac{y_2 - y_1}{b_2} = \frac{z_2 - z_1}{b_3} \tag{5}$$

$$x_2^2 + y_2^2 = [1 - z_2 \tan \alpha)\ a_2]^2 \tag{6}$$

where $a_2 = r_2/R_0$ (Fig. 3). Eq. (5) describes the line along which light propagates in n_1 while Eq. (6) describes the conical surface, s_2, separating the shells with index n_1 and n_2.

The ray direction, $\vec{c}$ ($|c| = 1$) in the shell beyond s_2 is given by the solution of the generalized Snell's law

$$(n_1\vec{b} - n_2\vec{c}) \times \vec{p} = 0 \tag{7}$$

where $\vec{p}$ is the normal to s_2 at the point of intersection,

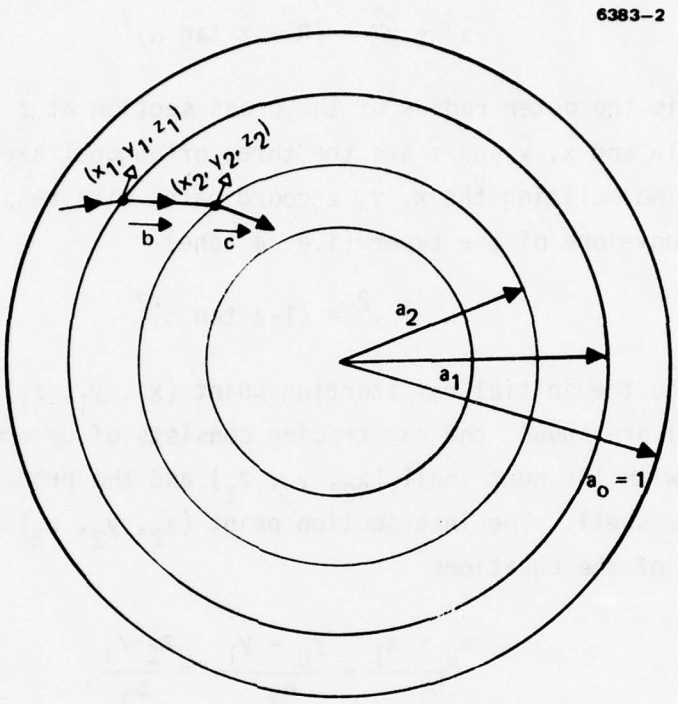

Fig. 3. Schematic representation of the normalized fiber shell dimensions and the ray definitions of the text.

$$\vec{p} = \cos(\delta)\frac{x_2}{\sqrt{x_2^2 + y_2^2}}\vec{i} + \cos(\delta)\frac{y_2}{\sqrt{x_2^2 + y_2^2}}\vec{j} + \sin(\delta)\vec{k} \tag{8}$$

with $\delta = \tan^{-1}(a_2 \tan\alpha)$. Eq. (7) indicates that the linear combination $n_1\vec{b} - n_2\vec{c}$ is along the normal $\vec{p}$ or that

$$n_2\vec{c} = n_1\vec{b} + \Gamma\vec{p} \tag{9}$$

where Γ is a constant. By squaring Eq. (9) and using the condition $|\vec{c}| = |\vec{b}| = |\vec{p}| = 1$ a quadratic in Γ is obtained. The physically reliazable solution for $\vec{c}$ is given by the value of Γ with the smallest magnitude. The two values of Γ are given by

$$\Gamma = -n_1\vec{b}\cdot\vec{p} \pm \sqrt{(n_1\vec{b}\cdot\vec{p})^2 - n_1^2 + n_2^2} \tag{10}$$

The solution of Eqs. (5)-(6) and (9)-(10) determines the ray after the surface s_2; the procedure can be repeated until the ray emerges from the fiber.

A computer program based on the above analysis has been used to analyze the optical properties of tapered fibers. The results for a solid single index fiber (no cladding) with index n = 1.46 (silica) and taper angles .5°, 1°, and 2° are shown in Fig. 4. These curves confirm the experimental data of Fig. 1. Since the curves are identical in shape, only data for a 1° taper is presented below.

Figure 5 shows the deflection angle vs. the azimuth angle for three cases:

a) a uniform fiber with n = 1.46

b) a clad fiber with $n_{core} = 1.50$ and $n_{clad} = 1.46$ (2.7% difference between core and cladding) and $r_{core}/r_{clad} = .5$

c) same as b except $r_{core}/r_{clad} = .667$.

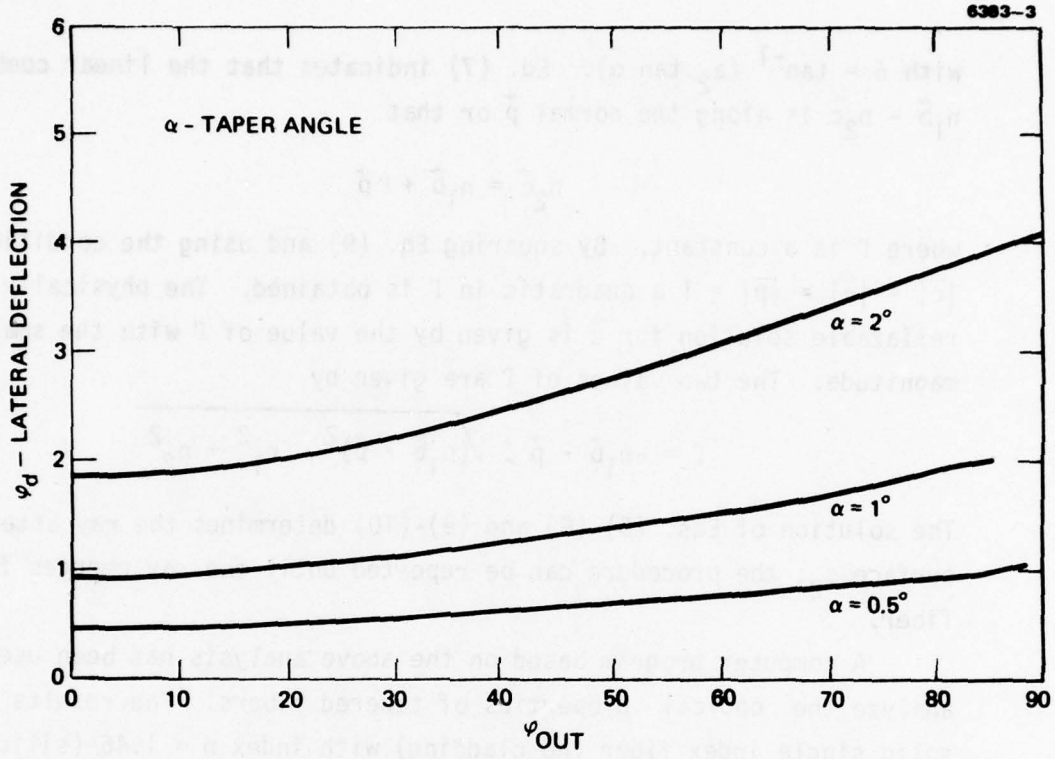

Fig. 4. Analytically determined lateral deflection angle versus the azimuth angle of the outgoing ray for a solid single index fiber and taper angles .5°, 1° and 2°.

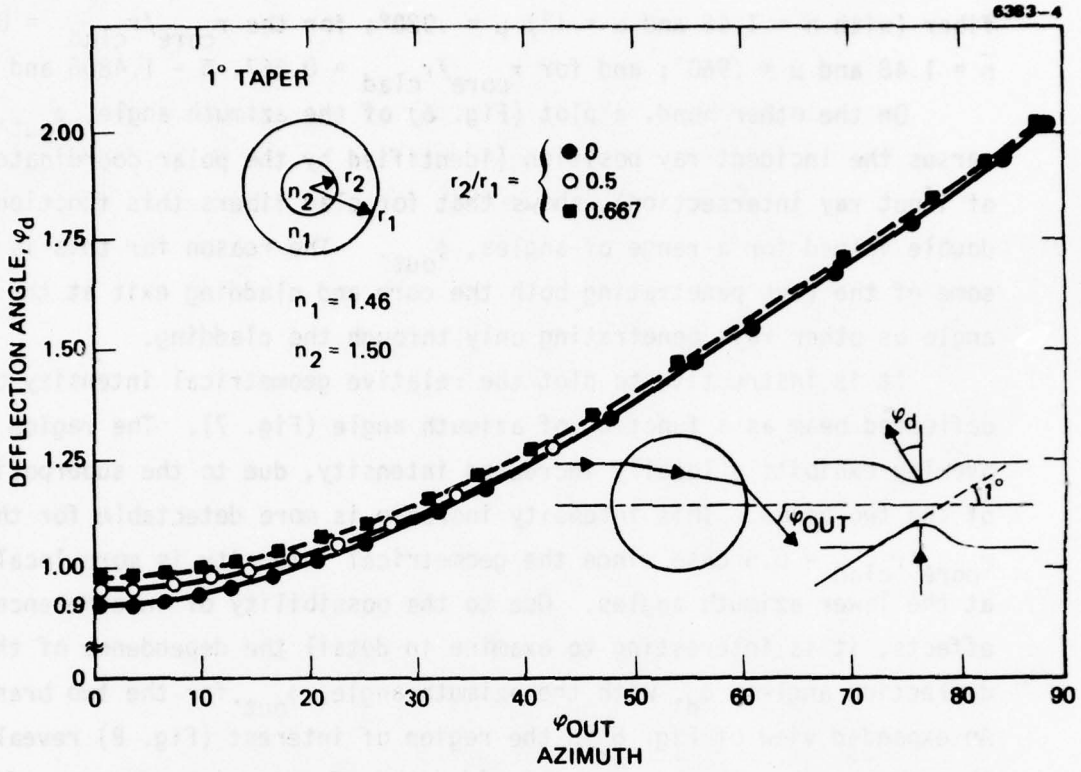

Fig. 5. Analytically determined lateral deflection angle versus the azimuth angle of the outgoing ray for three clad fibers.

It is clear that the deflection angle doesn't give any easy identification of the fiber's internal structure. The paraxial deflection angle is indeed the one predicted by Eq. (1) in conjunction with Eq. (2). For the uniform fiber (with n = 1.46 and α = 1°) μ = .920°; for the r_{core}/r_{clad} = 0.5, $\bar{n}$ = 1.48 and μ = .960°; and for r_{core}/r_{clad} = 0.667, $\bar{n}$ = 1.4866 and μ = .973°.

On the other hand, a plot (Fig. 6) of the azimuth angle, ϕ_{out}, versus the incident ray position (identified by the polar coordinate, ϕ_{in}, of input ray intersection), shows that for clad fibers this function is double valued for a range of angles, ϕ_{out}. The reason for this is that some of the rays penetrating both the core and cladding exit at the same angle as other rays penetrating only through the cladding.

It is instructive to plot the relative geometrical intensity of the deflected beam as a function of azimuth angle (Fig. 7). The region of overlap exhibits a locally increased intensity, due to the superposition of the two beams. This intensity increase is more detectable for the r_{core}/r_{clad} = 0.5 case since the geometrical intensity is more localized at the lower azimuth angles. Due to the possibility of interference effects, it is interesting to examine in detail the dependence of the deflection angles, ϕ_d, with the azimuth angle, ϕ_{out}, for the two branches. An expanded view of Fig. 5 in the region of interest (Fig. 8) reveals that the two branches do not coincide; therefore no interference effect is exhibited. One thus should be able to measure a variation in the intensity of the deflected beam indicative of the refractive index profile of the fiber cross section. Measurements of this type will be conducted during the next reporting period.

2. Modal dependence of the insertion loss of taper couplers

In the last contract status report, the insertion loss of taper couplers exposed to air versus the modal index was reported. In the experiment, a tapered optical fiber was butt coupled to a short pigtail of fiber on which a glass coupling prism was pressed. When the two fibers are aligned properly, there is no mode mixing at the butt joint. The output power after the tapered section was measured as different groups of modes were excited by changing the prism coupling angle. Then the tapered fiber was cut near the butt joint so that the input power

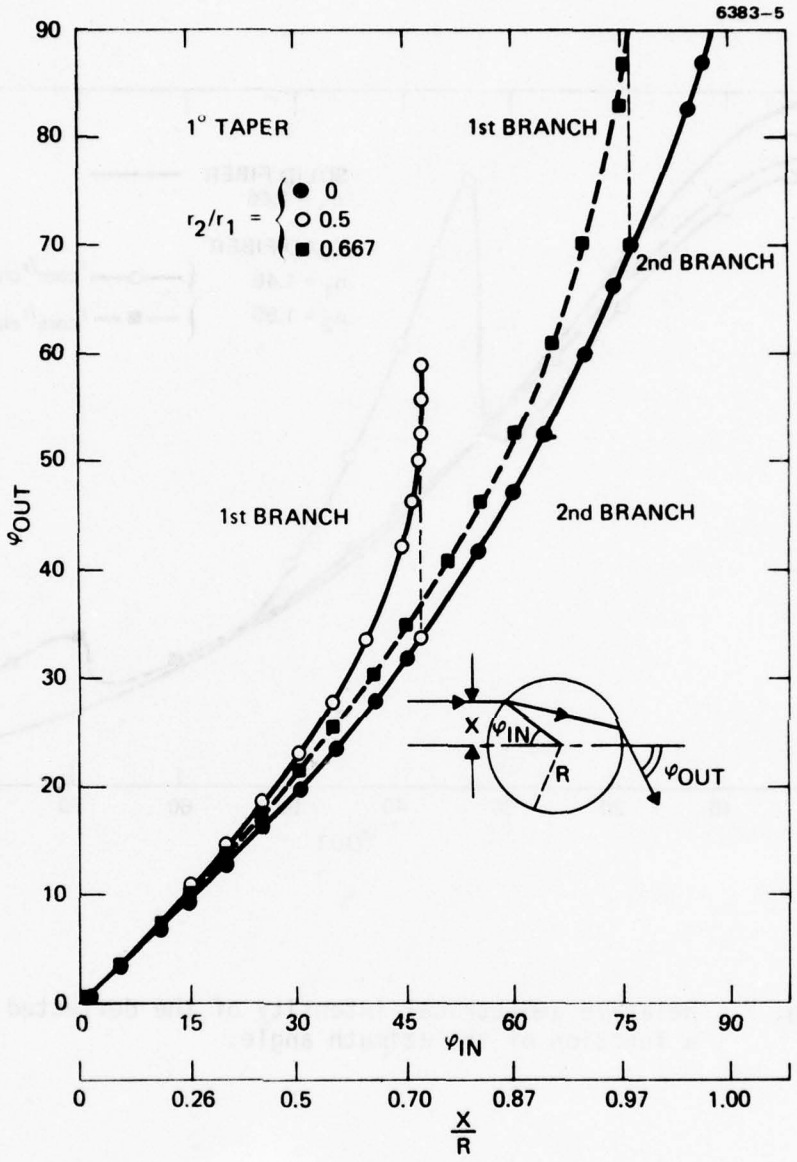

Fig. 6. Analytically determined azimuth angle versus the incident ray position.

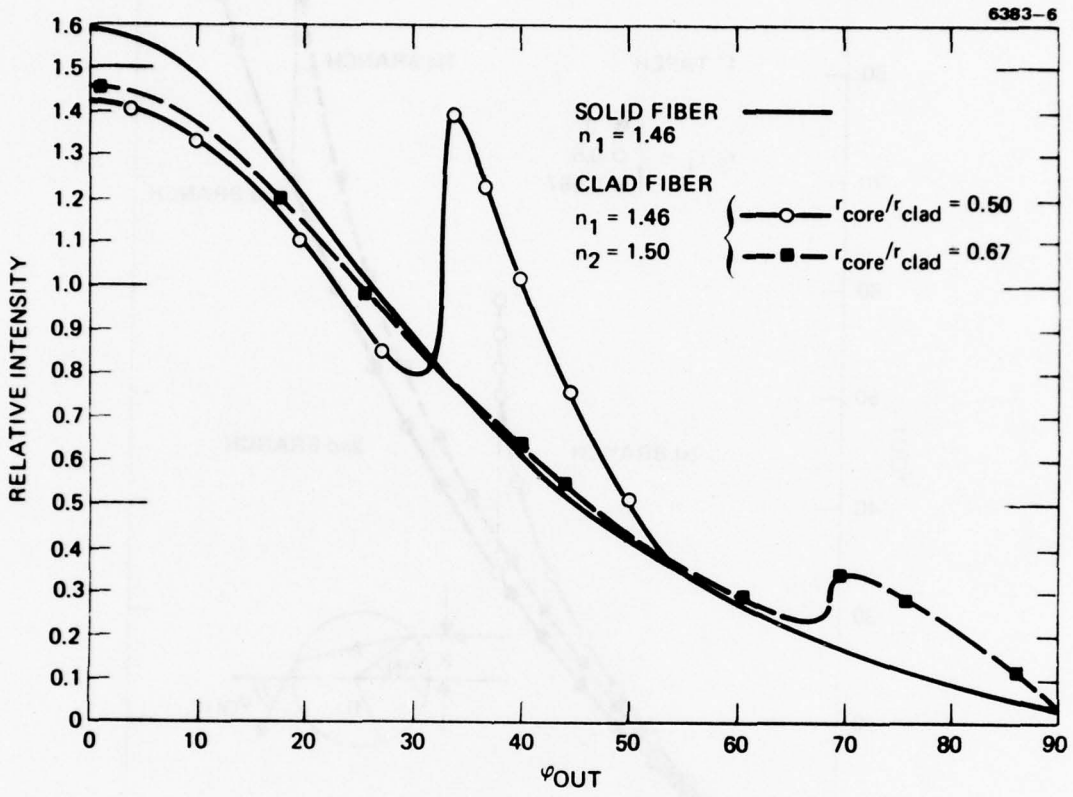

Fig. 7. Relative geometrical intensity of the deflected beam as a function of the azimuth angle.

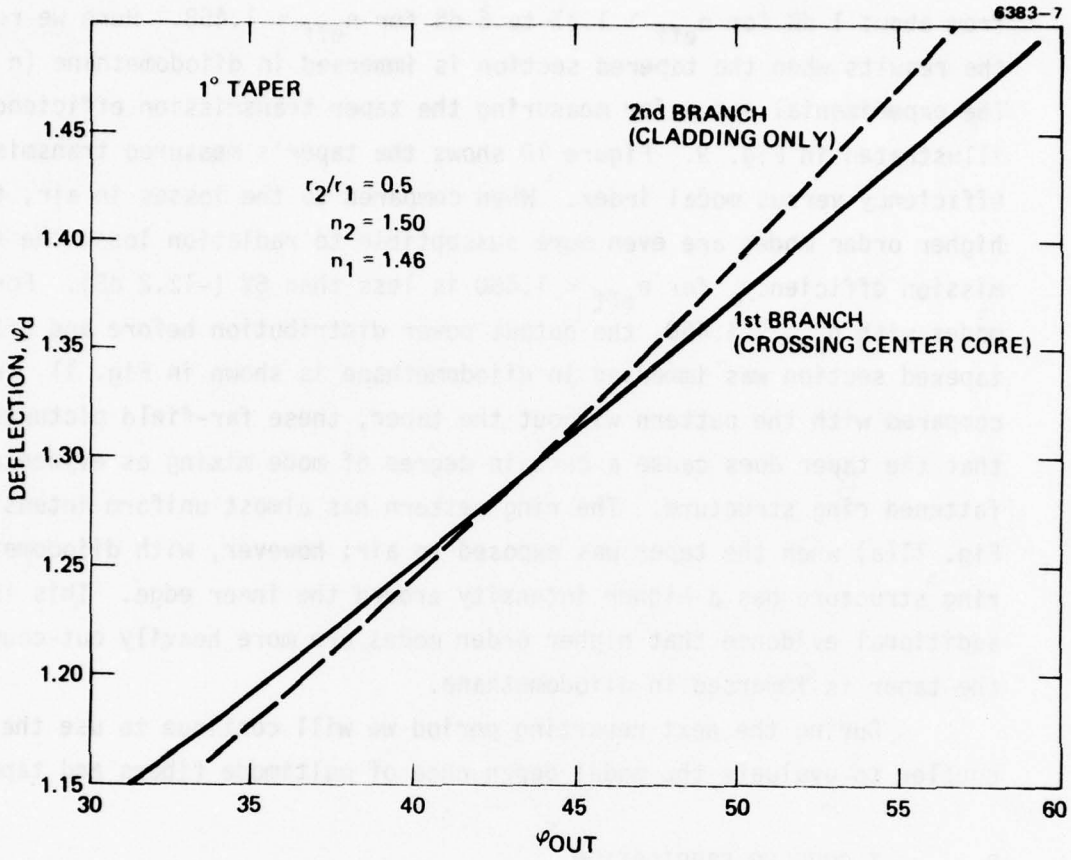

Fig. 8. Analytically determined lateral deflection angle versus the azimuth angle of the outgoing ray for the case indicated.

could be measured in a similar fashion. The ratio of the output to input power is defined as the insertion loss of the taper. When the tapered section was exposed to air, the insertion loss of the tapered fiber increases from about 1 dB for $n_{eff} \sim 1.47$ to 6 dB for $n_{eff} \sim 1.458$. Here we report the results when the tapered section is immersed in diiodomethane ($n = 1.74$). The experimental setup for measuring the taper transmission efficiency is illustrated in Fig. 9. Figure 10 shows the taper's measured transmission efficiency versus modal index. When compared to the losses in air, the higher order modes are even more susceptible to radiation loss; the transmission efficiency for $n_{eff} \lesssim 1.460$ is less than 6% (-12.2 dB). For fiber modes with $n_{eff} \lesssim 1.460$, the output power distribution before and after the tapered section was immersed in diiodomethane is shown in Fig. 11. When compared with the pattern without the taper, these far-field pictures indicate that the taper does cause a certain degree of mode mixing as evidenced by a fattened ring structure. The ring pattern has almost uniform intensity in Fig. 11(a) when the taper was exposed to air; however, with diiodomethane, the ring structure has a higher intensity around the inner edge. This is an additional evidence that higher order modes are more heavily out-coupled when the taper is immersed in diiodomethane.

During the next reporting period we will continue to use the prism coupler to evaluate the modal dependence of multimode fibers and tapers.

B. T-COUPLER FABRICATION

During this reporting period two construction techniques have been investigated. The first is the welding or fusing or fibers in the curved fixture with a CRL Model 42 CO_2 laser. The second technique is the lapping of fibers such that the lapped and polished sections can be either welded or epoxied together; the welding is done with a 2W CO_2 laser.

The fusing of fibers in the curved fixture has proved to be unrewarding. The basic problem arises in the following manner. At the position where the weld is desired the fibers are pressed against the fixture in order to insure contact of the fibers. This produces a very efficient and localized heat sink. However, a short distance away the fibers are not pressed against the fixture and upon heating tend to distort, pull away from the fixture, and move together. This motion is due to the stresses in the fibers, and results in a junction similar to that shown in Fig. 12(a). The desired

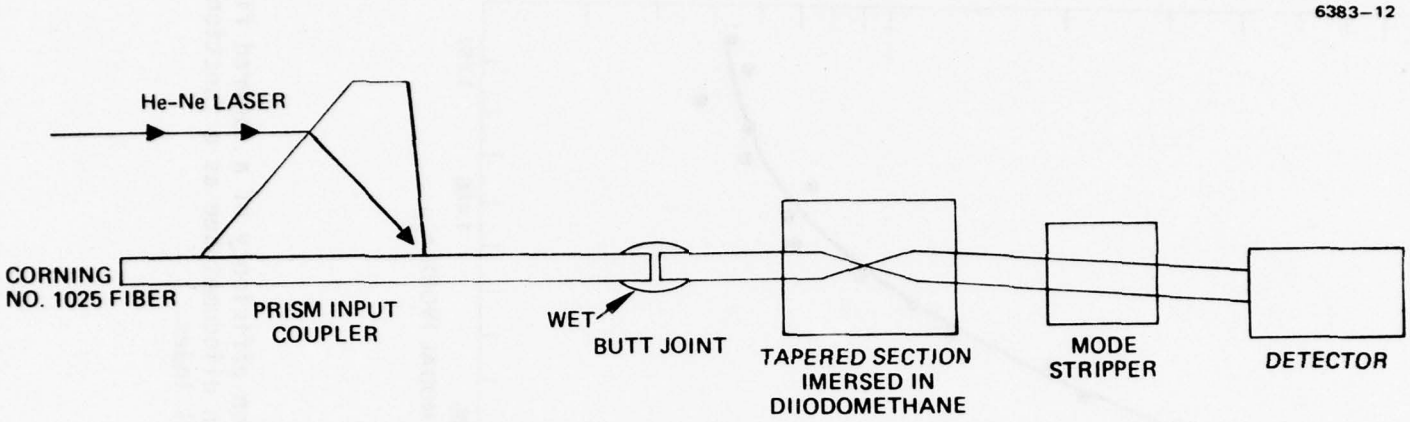

Fig. 9. Experimental setup for insertion loss measurement of tapered fibers.

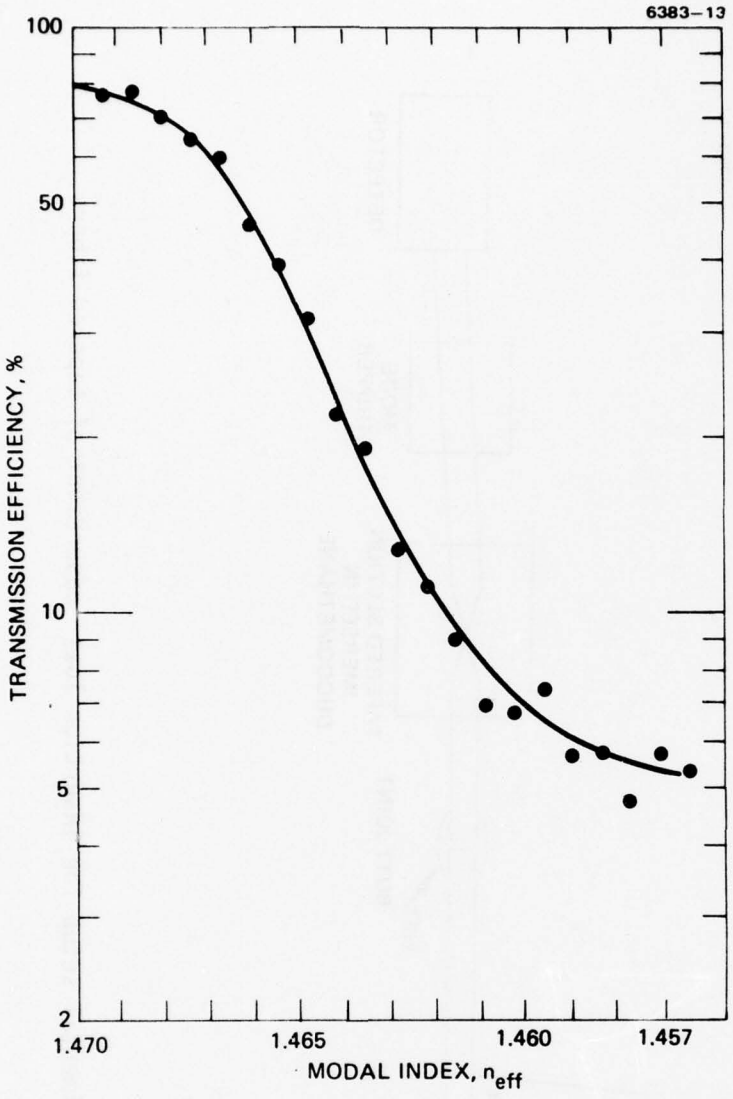

Fig. 10. Transmission efficiency of a tapered fiber immersed in diiodomethane as a function of fiber modal index.

6383-14

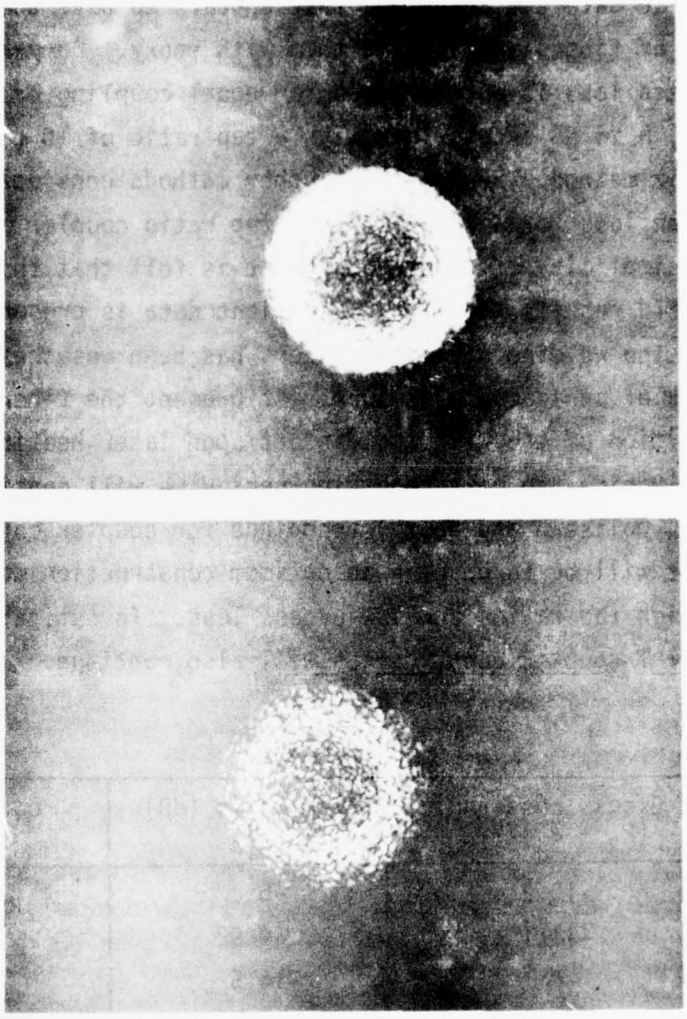

(a)

(b)

Fig. 11. Far field pattern of higher order modes ($n_{eff} \sim 1.460$) when the tapered fiber was a) exposed to air, b) immersed in diiodomethane.

structure is shown in Fig. 12(b). That is, the end result is a distorted contact with little hope of being controlled with the present fixture. Another problem with this technique has been the low yield of usable junctions (<10% of attempts). A spectrum of the typical values for excess loss and tap ratio are shown in Table I. In general a low tap ratio coupler has a high excess loss.

To date the technique that appears to have the best promise is the lapping of fibers and joining them with epoxy. Compared to other techniques the excess loss is much reduced for equal coupling or tap ratio. For example, a .5 dB excess loss with a tap ratio of 10 dB has been obtained with this method. From all the other methods considered to date, the lowest insertion loss for a 10 dB or less tap ratio coupler has been 1.8 dB. Due to the simplicity of construction, it is felt that this technique will give repeatable results; however, sufficient data is presently not available.

The welding of lapped fibers has been unsuccessful. This is due to the lack of an adequate fixture. At present the fibers are unsupported at the position of the weld and distort upon laser heating.

During the next reporting period we will continue to develop the LPE (lapped, polished and epoxy) technique for coupler construction. The primary emphasis will be to develop an optimum construction method which consistently gives high tap ratios and low excess loss. Investigation of the other methods of fiber T-coupler construction will also continue.

TABLE I

Excess Loss (dB) $(P_3 + P_4)/P_1$	Tap Ratio (dB) P_3/P_4	Corning Fiber
-13.2	-5	#1025
-11.1	-4.92	#1025
-8	-14.5	#1025
-4.9	-6.7	#1025
-1.5	-19.3	#1025

6438-1

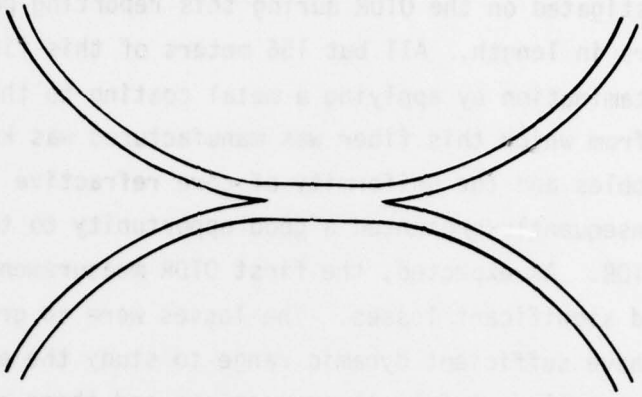

a. CHARACTERISTIC SHAPE OF FIBER WELD. THE TYPICAL WELD HOWEVER IS MUCH MORE DISTORTED IN SHAPE.

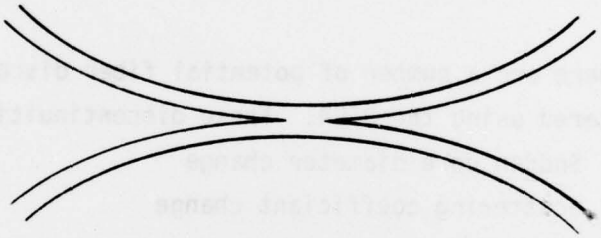

b. DESIRED FIBER WELD.

Fig. 12. Schematic representation obtained in the curved fixture.

C. FIBER PARAMETER STUDIES

Hughes Research Laboratories is engaged in the development and testing of high tensile strength glass fibers. The first of these fibers was investigated on the OTDR during this reporting period. The fiber was 539 meters in length. All but 156 meters of this fiber had been protected from contamination by applying a metal coating to the fiber. The preform from which this fiber was manufactured was known to contain many small bubbles and the uniformity of core refractive index was suspect. This fiber consequently presented a good opportunity to test the capabilities of the OTDR. As expected, the first OTDR measurement indicated that the fiber had significant losses. The losses were so great that the OTDR did not have sufficient dynamic range to study the entire fiber. The fiber was subsequently cut into three sections and these sections examined individually. The results of these measurements are listed in Table II. A semi-logarithmic plot of the detected waveform from the center section of fiber (partially metal clad) is shown in Fig. 13. There are two striking features of this waveform. First, there is an increase in the detected signal power as the probe pulse enters the metal-coated section of fiber. Second, there is a region of very high loss just within the metal-coated region.

There are a number of potential fiber discontinuities which might be encountered using the OTDR. These discontinuities include:

- Sudden core diameter change
- Scattering coefficient change
- NA change
- Lossy coating introduction
- Simple dielectric discontinuity (crack or bubble).

We know from previous work that the detected Rayleigh scattered power is given by Eq. (I-4). Using this expression, we can attempt to explain the behavior of the center section of the HAC fiber. This section can be divided into four distinct regions, each of different loss characteristics. The first region of 20 m exhibits the lowest loss, 29 dB/km. Since the

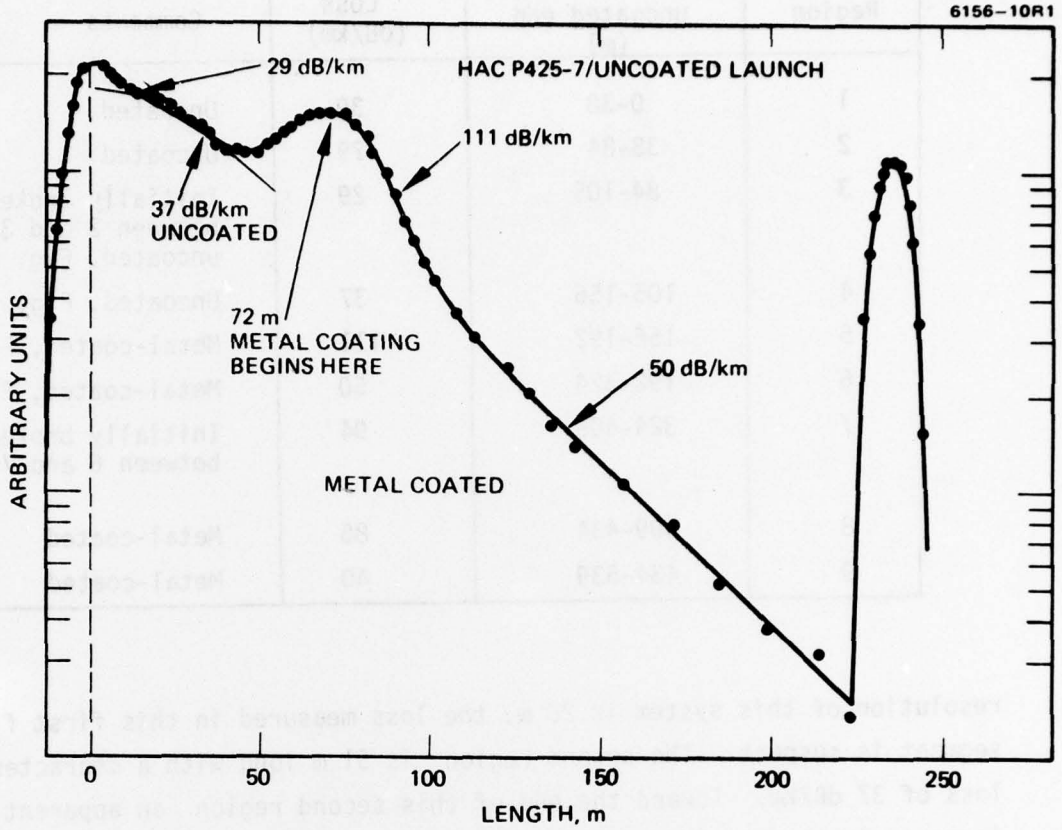

Fig. 13. A semi-logarithmic plot of the detected waveform from the center section of HAC fiber (partially metal clad).

TABLE II

TDR Results on HAC P425-7

Region	Distance from uncoated end (m)	Loss (dB/km)	Comments
1	0-38	39	Uncoated
2	38-84	29	Uncoated
3	84-105	29	Initially broken between 2 and 3 uncoated, Fig. 13
4	105-156	37	Uncoated, Fig. 13
5	156-192	111	Metal-coated, Fig. 13
6	192-324	50	Metal-coated, Fig. 13
7	324-409	94	Initially broken between 6 and 7
8	409-434	86	Metal-coated
9	434-539	40	Metal-coated

resolution of this system is 26 m, the loss measured in this first fiber segment is suspect. The second region is 51 m long with a characteristic loss of 37 dB/km. Toward the end of this second region an apparent increase in the returned signal occurs, bringing us into the third loss region 36 m long exhibiting a very high loss, 111 dB/km. The fourth region is 132 m long and 50 dB/km. The discontinuity 20 m down the fiber exhibits very little excess loss. It does, however, appear to mix the probe-pulse power distribution into higher order modes, accounting for the higher loss in the second region. Since the taper coupler couples power into high order modes as well as leaky modes, we expect a large portion of the power is in leaky modes following the first discontinuity. Since the size of this discontinuity appears to be about the same as the probe pulse length, we expect this is a bubble or crack.

The apparent increase in signal at the second discontinuity is postulated to be a change in the scattering coefficient, α_s. Note that the location of this discontinuity corresponds with the position where the metal coating begins. We know that these early experimental fibers suffered additional mode mixing caused by microbending. This observation is consistent with the present assumption of a step change in scattering coefficient. In addition, Eq. (I-4) suggests that the magnitude of the apparent signal gain should be the ratio of the two scattering coefficients. As the probe pulse starts into the discontinuity, the signal amplitude is 115 (arbitrary units) and as it just gets into the third region, the amplitude is 155. The ratio is 1.35. The scattering coefficient α_s (as determined by a least-square exponential curve fit of the data) in region two is -16.92/km and -23.12/km in region three. The ratio of these two coefficients is 1.37, in good agreement.

The extremely high loss in region three (111 dB/km) is attributed to the attenuation of leaky and higher order mode power caused by the lossy metal coating in the fiber. Additional evidence supporting this statement is found in the measured effective NA in the uncoated and coated sections. Following the coated section the effective NA is reduced significantly (36%) over the effective launch NA.

A more recently manufactured fiber has a measured loss of 7.2 dB/km in the uncoated section and 12.1 dB/km in the metal-coated section, both of these measurements are at an optical wavelength of 0.9 μm. At 0.82 μm the losses have been measured to be approximately 2 dB less than the losses at 0.9 μm. This fiber development is being done on another contract.

In addition to the above, an effort has been made to extend the effective range of the OTDR. One pertinent application of this long length OTDR is an evaluation of the steady state mode mixing length predicted by Olshansky et al.[1] A 4-km section of multimode graded index silica fiber purchased on this contract has arrived and is available for these experiments. The taper coupler OTDR described in a previous report has a range of 1.8 km in this fiber. In order to obtain conclusive results, this maximum distance must be increased.

Three tries have been made to extend the range of the OTDR measurements. First, the .9 μm GaAs laser source previously used was replaced with a GaAlAs laser (λ = .82 μm). At this new wavelength the absorptive contribution to the loss is significantly less; however, the peak output power of the available device is two orders of magnitude lower. It was hoped that the lower absorption and the smaller size (higher brightness) would compensate for the lower power; however, the overall result was that the range was not improved.

The other two coupling methods tried involve new coupling schemes which have the potential of coupling more light into the fiber. The first technique uses a fiber optic "T" coupler which is coupled to the test fiber via a simple butt connection (Fig. 14). Initial experiments using a "T" coupler have failed due to a large amount of scattering in the coupler. Although this method has future potential, further investigation has been postponed until the "T" couplers are optimized.

The third technique has been somewhat more successful. This technique is illustrated in Fig. 15. An injection laser is collimated with a high NA microscope objective. This light is then polarized, using a prism polarizer, parallel to the plane of incidence with the beam splitter. The beam splitter is an ordinary .009 in. piece of glass, but it is set to be near the Brewster's angle so that the light may pass through it with very small reflections. This light is then focused on the fiber end with another microscope objective. The numerical aperture and focal length of this lens are chosen to match the fiber. The fiber itself is precisely located using a trumpet alignment tube, thus giving a quick and convenient way to exchange fibers. The optical power back scattered within the fiber is recollimated and reflected off the beam splitter. A second polarizer is crossed with respect to laser polarizer. This blocks spurious reflections such as the 4% Fresnel reflection from the fiber end. Finally, the back scattered light from the fiber is focused on an avalanche photodiode, which is used to detect the signal. Since the polarization of the detected light is normal to the plane of incidence of the beam splitter, it does not exhibit a Brewster condition and hence has a high reflectivity. The angle of the beam splitter has been chosen to maximize the signal received by the detector.

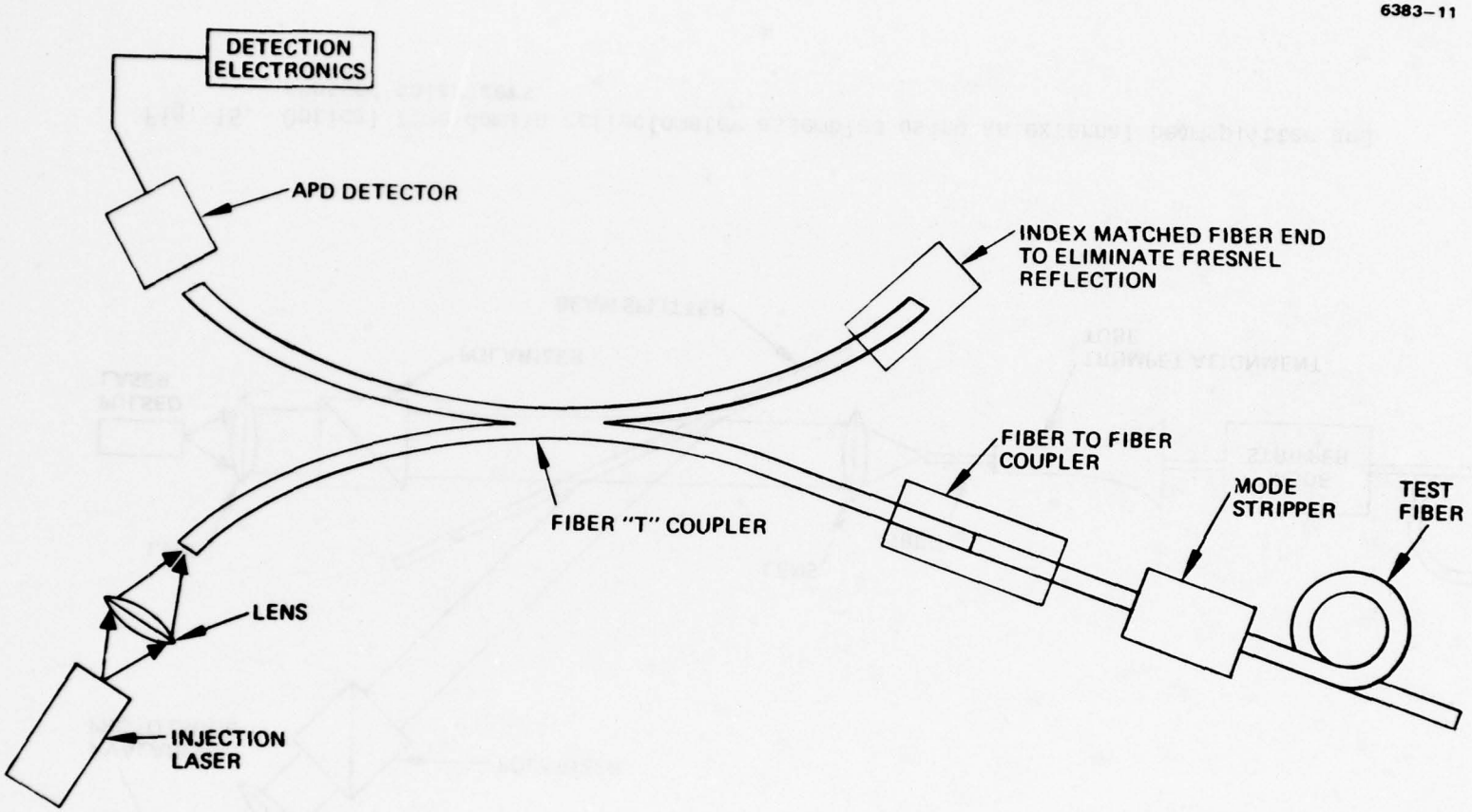

Fig. 14. Optical time domain reflectometer assembled using a fiber "T" coupler.

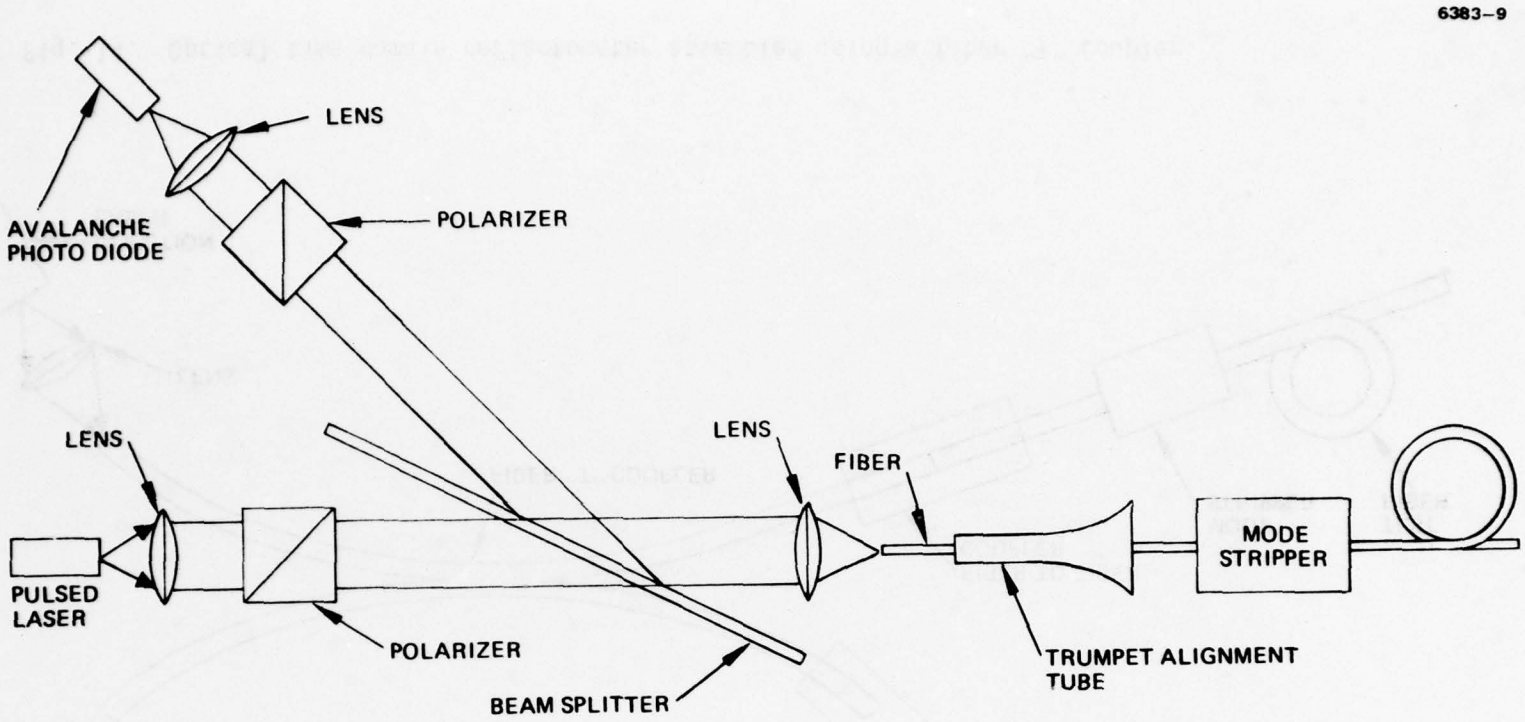

Fig. 15. Optical time domain reflectometer assembled using an external beamsplitter and crossed polarizers.

Calculations have shown that the transmission and reflection losses of the beam splitter are less than -3 dB when compared to the optimal case where the input laser beam is totally transmitted and back scattered beam totally reflected.

Finally, a comment must be made on the fact that we are detecting a polarization rotated by 90° from the input polarization. In multimode glass fibers the input light is depolarized within a short distance, much less than the present resolution of the OTDR (∿26 meters) and hence the OTDR measurements are unaffected by the polarization sensitive detection. In addition to this, the Rayleigh scattered light is itself depolarized and therefore even in single mode[6] or liquid core[7] fibers when the polarization is preserved over long lengths, this measurement technique will be useful.

Figure 16 shows the backscattered signal from the 4-km section of graded index multimode silica fiber obtained using this crossed polarizer technique. The entire return signal can be seen in Fig. 16(a). It is evident that the Fresnel reflection from the launch end of the fiber has been reduced to be within 5.5 dB of the Rayleigh scattered return. This demonstrates the effectiveness of the crossed polarizer technique for blocking reflections in the launching apparatus. Also evident in Fig. 16(a) is the Fresnel reflection from the fiber end (4.2 km away). Figure 16(b) is a 10x enlargement of Fig. 16(a). The exponential decay of the Rayleigh is clearly visible in Fig. 16(b). A small imperfection in the fiber is also visible in Fig. 16(b). This is evident by the small blip in the Rayleigh return approximately 1/3 of the way to the fiber end (∿1.5 km down the fiber). The origin of this imperfection is unknown at present. Unfortunately, we are only able to see a Rayleigh return from slightly over 2 km of fiber. Within this distance there is no conclusive evidence of a steady-state mode mixing length. Two possible explanations of this are: 1) the change in loss for the steady state mode mixing length is small and we must obtain a Rayleigh signal from longer lengths of fiber to observe it or 2) the small imperfection ∿1.5 km down the fiber scatters the light from a nearly steady state mode distribution effectively making the steady-state mixing length longer. An OTDR measurement from the other end of the fiber has not been done due to the inaccessibility of that end. However, during the next reporting period

6383-10

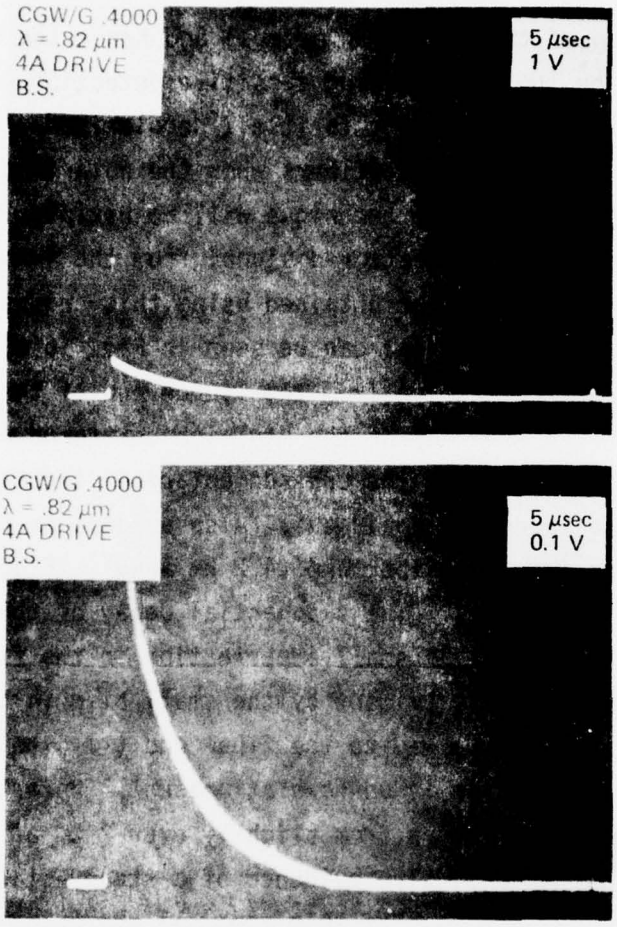

Fig. 16. a) Oscillogram of the deflected backscattered light from a 4-km fiber using the external beamsplitter technique. The time scales are 5 μsec per division.
b) 10x enlargement of a).

this end will be made accessible and an OTDR measurement will be produced. In addition to this, the coupling scheme will be optimized and hopefully a Rayleigh return from more than 2 km of fiber will be observed.

REFERENCES

1. R. Olshansky, M. G. Blankenship, D. B. Keck, 2nd European Conference on Optical Fiber Communication, Paris (1976).
2. H. M. Presby, J. Opt. Soc. Am. 64, 200 (1974).
3. J. W. Y. Lit, J. Opt. Soc. Am. 65, 1311 (1975).
4. D. Marcuse, Appl. Opt. 14, 1528 (1975).
5. D. Marcuse, H. M. Presby, Paper PD2-1, Optical Fiber Transmission II, Mtg., Williamsburg, VA, Feb 1977.
6. A. Papp and H. Harms, Appl. Optics 16, 1315 (1977).
7. F. P. Kapron, N. F. Borelli, and D. B. Keck, J. Quant. Electr. QE-8, 222 (1972).

METRIC SYSTEM

BASE UNITS:

Quantity	Unit	SI Symbol	Formula
length	metre	m	...
mass	kilogram	kg	...
time	second	s	...
electric current	ampere	A	...
thermodynamic temperature	kelvin	K	...
amount of substance	mole	mol	...
luminous intensity	candela	cd	...

SUPPLEMENTARY UNITS:

plane angle	radian	rad	...
solid angle	steradian	sr	...

DERIVED UNITS:

Acceleration	metre per second squared	...	m/s
activity (of a radioactive source)	disintegration per second	...	(disintegration)/s
angular acceleration	radian per second squared	...	rad/s
angular velocity	radian per second	...	rad/s
area	square metre	...	m
density	kilogram per cubic metre	...	kg/m
electric capacitance	farad	F	A·s/V
electrical conductance	siemens	S	A/V
electric field strength	volt per metre	...	V/m
electric inductance	henry	H	V·s/A
electric potential difference	volt	V	W/A
electric resistance	ohm		V/A
electromotive force	volt	V	W/A
energy	joule	J	N·m
entropy	joule per kelvin	...	J/K
force	newton	N	kg·m/s
frequency	hertz	Hz	(cycle)/s
illuminance	lux	lx	lm/m
luminance	candela per square metre	...	cd/m
luminous flux	lumen	lm	cd·sr
magnetic field strength	ampere per metre	...	A/m
magnetic flux	weber	Wb	V·s
magnetic flux density	tesla	T	Wb/m
magnetomotive force	ampere	A	...
power	watt	W	J/s
pressure	pascal	Pa	N/m
quantity of electricity	coulomb	C	A·s
quantity of heat	joule	J	N·m
radiant intensity	watt per steradian	...	W/sr
specific heat	joule per kilogram-kelvin	...	J/kg·K
stress	pascal	Pa	N/m
thermal conductivity	watt per metre-kelvin	...	W/m·K
velocity	metre per second	...	m/s
viscosity, dynamic	pascal-second	...	Pa·s
viscosity, kinematic	square metre per second	...	m/s
voltage	volt	V	W/A
volume	cubic metre	...	m
wavenumber	reciprocal metre	...	(wave)/m
work	joule	J	N·m

SI PREFIXES:

Multiplication Factors	Prefix	SI Symbol
1 000 000 000 000 = 10^{12}	tera	T
1 000 000 000 = 10^{9}	giga	G
1 000 000 = 10^{6}	mega	M
1 000 = 10^{3}	kilo	k
100 = 10^{2}	hecto*	h
10 = 10^{1}	deka*	da
0.1 = 10^{-1}	deci*	d
0.01 = 10^{-2}	centi*	c
0.001 = 10^{-3}	milli	m
0.000 001 = 10^{-6}	micro	μ
0.000 000 001 = 10^{-9}	nano	n
0.000 000 000 001 = 10^{-12}	pico	p
0.000 000 000 000 001 = 10^{-15}	femto	f
0.000 000 000 000 000 001 = 10^{-18}	atto	a

* To be avoided where possible.

MISSION
of
Rome Air Development Center

RADC plans and conducts research, exploratory and advanced development programs in command, control, and communications (C^3) activities, and in the C^3 areas of information sciences and intelligence. The principal technical mission areas are communications, electromagnetic guidance and control, surveillance of ground and aerospace objects, intelligence data collection and handling, information system technology, ionospheric propagation, solid state sciences, microwave physics and electronic reliability, maintainability and compatibility.

Printed by
United States Air Force
Hanscom AFB, Mass. 01731